Effect of Non-Proportional Multiaxial Fatigue Loading on Micro Crack Initiation and Propagation of Ti-6Al-4V

H. NAKAMURA[1], M. TAKANASHI[1], T. ITOH[2], Y. SHIMIZU[3], M. WU[3]

[1] Structural Strength Department, Research Laboratory, IHI Corporation, 1, Shin Nakahara-Cho, Isogo-ku, Yokohama-shi, Kanagawa 235-8501, Japan
E-mail: hiroshi_nakamura_2@ihi.co.jp

[2] Division of Mechanical Engineering, Graduate School of Engineering, University of Fukui, 9-1, Bunkyo 3-chome, Fukui-shi, Fukui 910-8507, Japan
E-mail: itoh@u-fukui.ac.jp

[3] Graduate School of Engineering, University of Fukui

Abstract. This paper describes multiaxial low cycle fatigue crack behavior of Ti-6Al-4V under non-proportional loading. Strain controlled fatigue tests under proportional and non-proportional loadings at 90-degrees out-of-phase were carried out on Ti-6Al-4V tubular specimens at room temperature. As a result, fatigue lives under the non-proportional multiaxial loading, in which strain ranges were estimated by using Mises base strain, were approximately 1/10 of those of the proportional one. Observation on replica specimen showed that the micro cracks for the proportional loading propagated independently, but that the cracks for the non-proportional one grew with coalescence. In addition, the crack growth rates under the non-proportional loading were faster than those of the proportional one. Therefore, significant reduction on the fatigue life may be attributed to crack coalescence due to the increase in micro crack initiation and the crack growth acceleration because many slip systems were activated by non-proportional loading. The life reduction corresponds to a decrease in fatigue strength, so that the fatigue strength under non-proportional loading became about 7/10 of that for the proportional one.

INTRODUCTION

Ti-6Al-4V has been used for aero engine components because of its excellent specific strength and corrosion resistance. Mechanical structures such as the rotating aero engine components are routinely subjected to thermal stress and body force, and these cyclic loading situations cause multiaxial low cycle fatigue (LCF). It has been reported that the fatigue lives under the multiaxial LCF non-proportional loading, in which directions of principal axes are changed within a cycle, are seriously reduced and are accompanied by an additional strain hardening [1-15]. Several studies have indicated that there is material dependence between life reduction and additional strain hardening [3-7]. There are a few research papers which deal with the multiaxial fatigue of Ti alloy [16, 17], however, the fatigue behavior under the non-proportional loading has not been clarified yet. In this study, strain controlled fatigue tests were conducted on Ti-6Al-4V using proportional and non-proportional loadings. Observations on micro crack

initiation and propagation were carried out by replicating the specimen surface during the fatigue tests. The fracture mechanism under the non-proportional loading will be discussed in view of additional hardening, and micro crack initiation and propagation.

MATERIALS AND EXPERIMENTAL PROCEDURE

Table 1 shows the chemical composition of the Ti-6Al-4V used. The supplied material was subjected to the following heat-treatment: 960°C for 1h. → water-cooling, and 705°C for 2h. → air-cooling. The bimodal α and β microstructure was obtained after the heat treatment. Table 2 indicates the mechanical properties of the material at room temperature. The specimen configuration for fatigue tests is shown in Fig. 1. The dimensions of the specimen were 6.8mm for the parallel part, 9mm as the inner diameter, and 11mm as the outer diameter.

Table 1. Chemical composition of Ti-6Al-4V bar stock material in wt.%.

C	V	Al	N	Fe	O	H	Ti
0.002	4.16	6.30	0.004	0.16	0.20	0.006	Bal.

Table 2. Mechanical properties of Ti-6Al-4V alloy.

Elastic modulus (GPa)	0.2% Proof stress (MPa)	Tensile strength (MPa)
118	943	1017
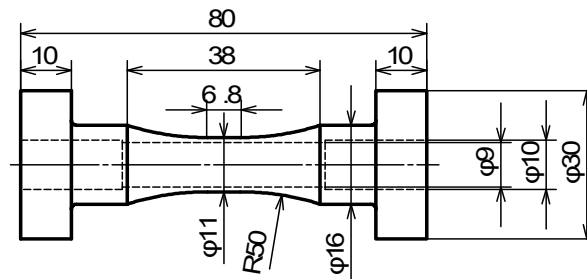
Figure 1. Geometry and sizes of the specimen (in mm).

Figure 2 shows strain paths in this study. There are two types of proportional paths. PP is the push-pull path, and TP is the torsion path. CP represents 90° out-of-phase loading which is the non-proportional path. Mises equivalent strain controlled tests, in which the strain rate of 0.1 or 0.5 %/s, were carried out at room temperature. The number of cycles to failure, N_f, was determined as the cycle at which the axial stress amplitude decreased by 25% from its cyclically stable value. To examine the additional hardening effect due to non-proportional loading, multiple step tests in which strains were increased were conducted. Strain paths for the multiple step tests were PP and CP at the strain rate of 0.1%/s. Information on micro crack initiation and propagation was

obtained by replicating the specimen surface with RepliSet (Struers A/S). Replication was performed for the specimens in which the Mises strain range $\Delta\varepsilon_{eq}$ was 1.2% for a selected number of cycles. The replicas were observed with a laser microscope (KEYENCE Corp., VK-9700), and were examined at a magnification of 400 times. At this magnification, a crack of 30μm was identifiable so that the crack initiation was defined as the crack length 2a of 30μm. The observed area was $2.5 \times 2.2\text{mm}^2$ centered in a critical crack leading to fatigue failure.
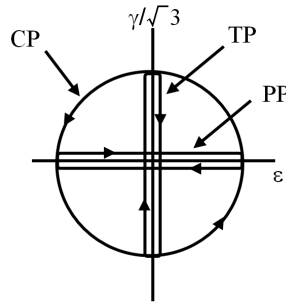
Figure 2. Strain paths on ε–$\gamma/\sqrt{3}$ plane in this study.

EXPERIMENTAL RESULT

Low cycle fatigue life and cyclic stress-strain relationship

Figure 3 shows the relationship between the Mises equivalent strain range and N_f. The solid line was the regression line based on the data of fatigue lives for PP, and the dashed lines show a factor of 2 scatter band. The fatigue lives for TP were within a factor of 2 scatter band. On the other hand, the fatigue lives for CP were approximately 1/10 of that for PP. In addition, the fatigue strengths for CP were about 7/10 of those of PP. Therefore, the non-proportional loadings caused significant life reduction of Ti-6Al-4V.
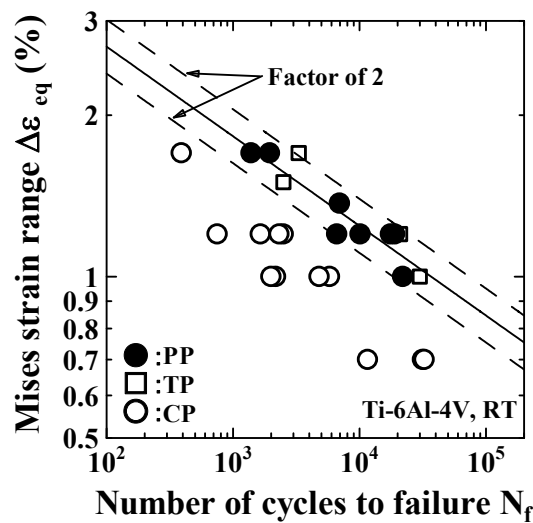
Figure 3. Mises equivalent strain range and number of cycles to failure.

Figure 4 indicates cyclic stress-strain relationship under PP and CP. Monotonic curve is also shown in this figure. Both axes present Mises stress and strain amplitude from hysteresis loop. The stress-strain relationship under PP and CP showed cyclic hardening compared to the monotonic curve. On the other hand, there was no deference between the stress-strain relationship under PP and that of CP. In general, fatigue life reduction is caused by non-proportional loading with an additional strain hardening [1-15]. Although Ti-6Al-4V under non-proportional loading had not shown any additional hardening effect, the fatigue lives were significantly reduced.
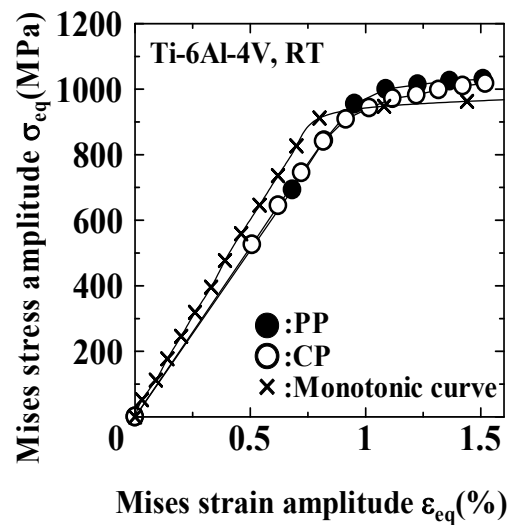
Figure 4. Cyclic stress-strain relationship in PP and CP.

Micro crack initiation and propagation behavior

The replicated cracks at the latter stage of the fatigue life are shown in Fig. 5. PP exhibited a few micro cracks around the critical crack in Fig. 5(a). The number of micro cracks was 8 in the observed area. On the other hand, TP showed about 40 micro cracks around the critical one in Fig. 5(b). Moreover, CP had much more micro cracks than those of PP and TP in Fig. 5(c). The number of cracks was more than 200.

Figure 6 indicates the number of micro cracks, which are classified into angle and length, as a function of the life ratio. The total number of cracks for PP increased with the life ratio in Fig. 6(a). Most cracks were oriented at an angle of $\pm 67.5°$ or $\pm 90°$ because they had propagated perpendicular to the principal stress direction. The number of long cracks augmented with the life ratio in Fig. 6(b), thus, each micro crack had grown independently.

Figure 6(c) shows that the total number of cracks for TP increases until $N/N_f=0.91$, and then the number decreases slightly. The number of cracks longer than 200 μm increased with the life ratio, but the number of cracks from 100 to 200 μm in length decreased at $N/N_f=0.97$ in Fig. 6(d). This result indicates that crack coalescence had occurred at the latter stage of the fatigue life. Figure 6(c) shows that micro cracks tend to propagate at $\pm 90°$, and that they grow at other angles as well. From this result,

Axial direction   1mm

(a) PP: N=10000(N/N$_f$=0.99)   (b)TP: N=20400(N/ N$_f$=0.97)   (c) CP: N=2100(N/ N$_f$ =0.91)
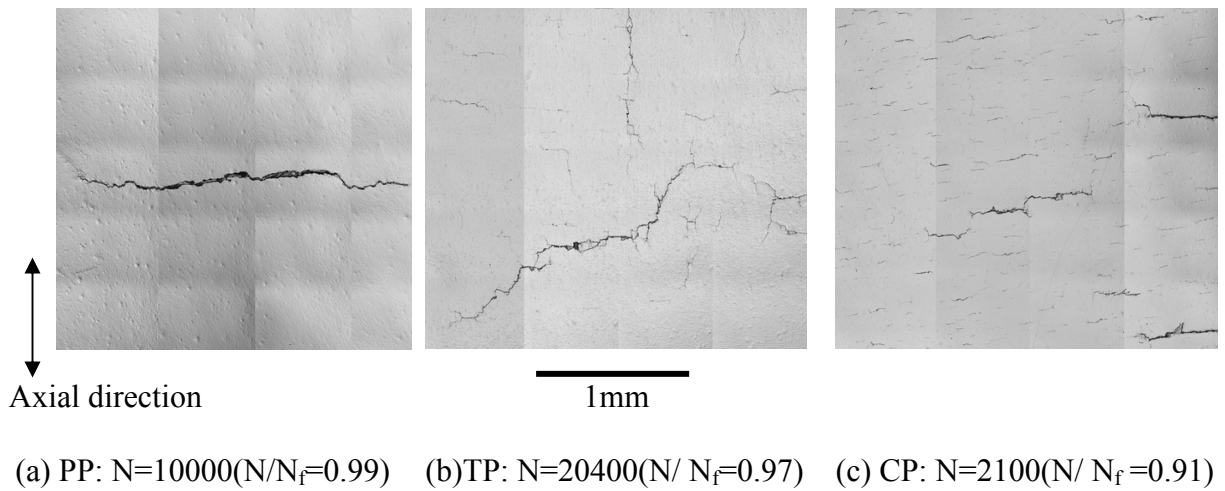
Figure 5. The critical cracks leading to fatigue failure.

the cracks for TP had grown primarily under Mode II and secondarily under Mode I.

The total number of cracks for CP indicates the local maximum at N/N$_f$=0.65 in Fig. 6(e). After that, the number decreased once and then increased again. This tendency could be seen particularly in the number of cracks shorter than 100μm in Fig. 6(f). Thus, the crack coalescence for CP had started in the middle stage of the fatigue life. Figure 6(e) shows that most cracks are oriented at angles of ±67.5° or ±90° so that the micro cracks for CP had propagated perpendicular to the maximum principal stress direction in a cycle.

Figure 7(a) represents the critical crack length versus the number of cycles. For PP, the critical crack longer than 30μm was observed on the replica at 500 cycles and N/N$_f$ was 0.05 at this time. The crack for PP propagated slowly during most of the fatigue life. The crack for TP longer than 30μm was seen at 2000 cycles, and N/N$_f$ was 0.1. The crack growth behavior was almost same as that of PP. For CP, the crack longer than 30μm was also shown at 500 cycles, and N/N$_f$ was 0.05. These results suggest that the crack initiation lives did not differ significantly between proportional and non-proportional loadings. However, the critical crack for CP propagated faster than those of PP and TP.

Figure 7(b) shows the crack growth rate da/dN versus stress intensity factor ΔK. The ΔK were calculated with $\Delta K = \Delta\sigma\sqrt{\pi a}$, where "a" was half the length of the critical crack. The crack which had propagated independently was used for the calculation. For PP and CP, principal stress amplitude was used because the crack had grown perpendicular to the maximum principal stress direction in a cycle. For TP, the critical crack had propagated under Mode II, so that principal shearing stress amplitude was used. There were no differences between the crack growth rates for PP and those of TP in Fig. 7(b). However, the crack growth rates for CP were approximately 10 times faster than those of PP and TP at which ΔK were larger than 10MPa√m.

491
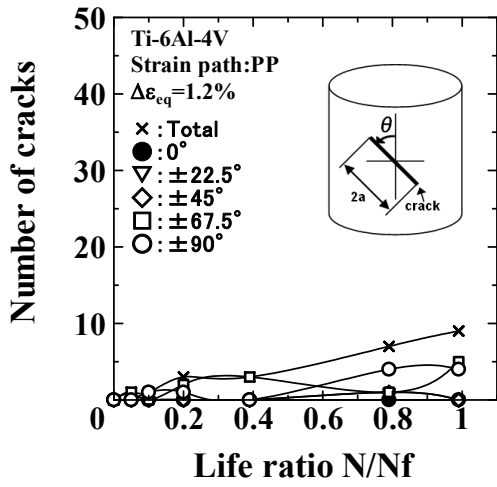
(a) Crack for PP classified into angle.
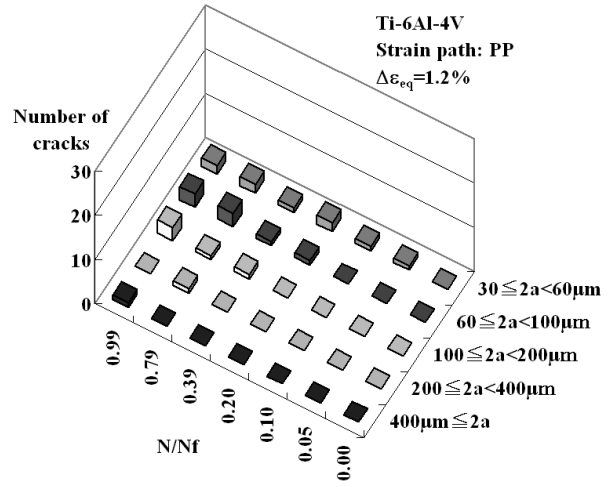
(b) Crack for PP classified into length.
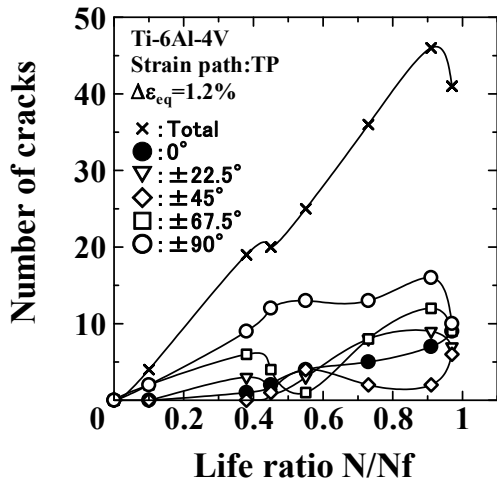
(c) Crack for TP classified into angle.
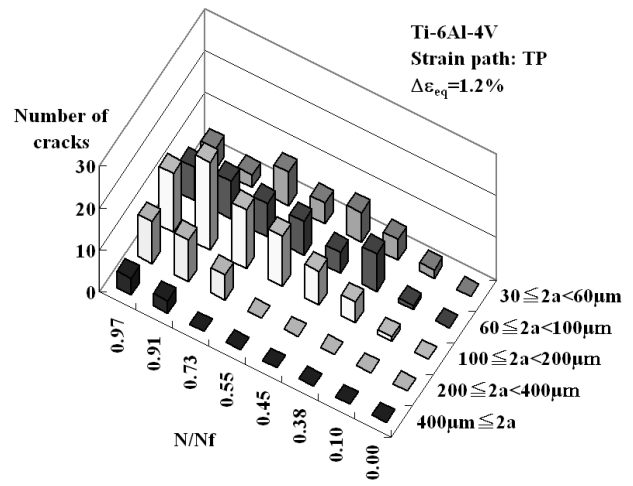
(d) Crack for TP classified into length.
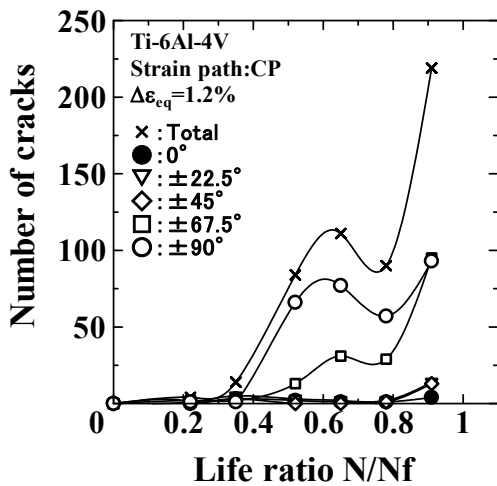
(e) Crack for CP classified into angle.
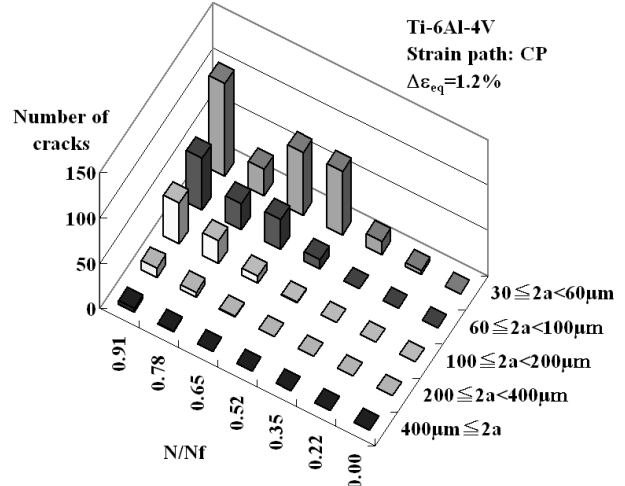
(f) Crack for CP classified into length.

Figure 6. Number of fatigue cracks as a function of life ratio.
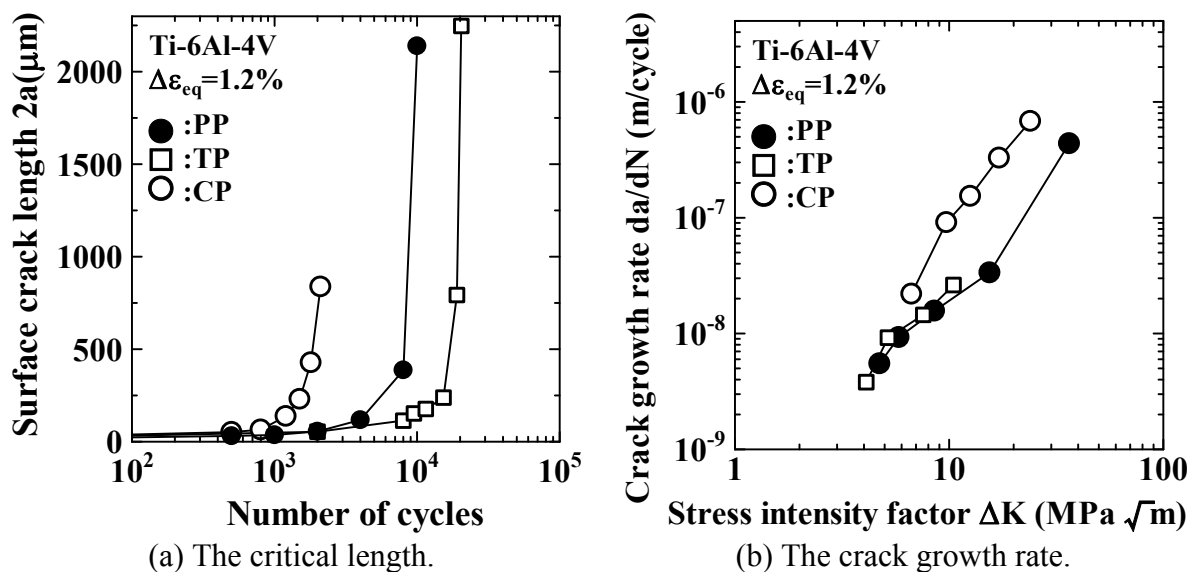
(a) The critical length.   (b) The crack growth rate.
Figure 7. The critical crack propagation behavior.

DISCUSSION

The replica observations for Ti-6Al-4V showed that there were 10 times more cracks for CP than those of PP after N/N_f =0.5. The micro cracks for PP had propagated independently. On the other hand, the cracks for CP had grown accompanied by coalescence. These results indicate that the micro cracks for CP have coalesced alternately after the middle of life. The crack initiation lives did not differ among PP, TP, and CP, however, the crack growth rates for CP were approximately 10 times faster than those of PP and TP.

Previous studies have shown that non-proportional loading activates more slip systems than proportional loading because the principal stress or strain axes are rotated during a cycle [1-5]. Activated slip systems by the non-proportional loading results in nucleating many micro cracks [3]. Thus, CP stimulated many slip systems for Ti-6Al-4V, and micro cracks initiated more than those of PP and TP. In addition, the microstructure was more damaged when a lot of slip systems were stimulated, so that the crack growth rates for CP were approximately 10 times faster than those of PP and TP. Moreover, if the critical crack coalesced at an early stage of life, the fatigue lives would be decreased to a greater extent. This suggests that the dispersion shown in the fatigue lives for CP may be caused by the crack coalescence. Consequently, the fatigue lives of Ti-6Al-4V for CP were approximately 1/10 of those of PP and TP. The life reduction corresponds to a decrease in fatigue strength, so that the fatigue strength for CP was about 7/10 of that for PP and TP. Therefore, significant life reduction shown in Ti-6Al-4V under non-proportional loading may be attributed to the crack coalescence due to an increase in micro crack initiation and the crack growth rate acceleration because of many activated slip systems.

Although there were about 5 times more cracks for TP than those of PP, fatigue lives did not differ seriously. For TP, crack coalescence occurred at the latter stage of life, and crack growth rates were almost the same as that of PP. Thus, the crack density for TP was not significant enough to affect fatigue life.

CONCLUSION

This paper focused on the fatigue crack behavior of Ti-6Al-4V under non-proportional loading. The fatigue lives under non-proportional loading were approximately 1/10 of those of the proportional one. Observations on micro cracks showed that there were 10 times more cracks for CP than those of PP after N/N_f=0.5. For PP, the micro cracks propagated independently, however, the crack coalescence had occurred for CP. The crack initiation lives did not differ among PP, TP, and CP, while on the other hand, the crack growth rates for CP were about 10 times faster than those of PP and TP. Thus, the significant reduction of fatigue life may be caused by the crack coalescence due to the increase in micro crack initiation and the accelerated crack growth rate because many slip systems were activated by the non-proportional loading. The life reduction corresponds to a decrease in fatigue strength, so that the fatigue strength of Ti-6Al-4V under non-proportional loading became about 7/10 of that for the proportional one.

REFERENCE
1. Socie D., Marquis G. (2000) Multiaxial Fatigue, SAE Int.
2. Doong SH., Socie DF., and Robertson IM. (1990) Trans ASME J Eng Mat Tech、 **112**, 456–464.
3. Itoh T., Murashima K., and Hirai T. (2007) J Soce Mat Sci, **56** 157-163.
4. Kida S., Itoh T., Sakane M., Ohnami M., and Socie DF. (1997) Fatigue Fract Eng Mat Struct, 20-10, pp.1375-1386.
5. Yang T. and Itoh T. (2008) Proc. LCF6, CD.
6. Itoh T., Nakata T., Sakane M., and Ohnami M. (1997) Proc. 5th Int. Conf. Biaxial/Multiaxial Fatigue Fracture, vol. I. 173–87.
7. Itoh T., Sakane M., Ohnami M., and Socie D F. (1995) J Eng Mat Tech **117**, 285-292.
8. Kanazawa K., Miller KJ., and Brown MW. Fatigue Eng Mater Struct, **2**, 217–228
9. GO H., ChShu C., and Gao Q. (1999) Proc. 7th Int. Fatigue Cong., vol. I. 917–922.
10. Chen X., An K., and Kim KS. (2004) Fatigue Fract Eng Mater Struct, **27**, 439–448.
11. Chen X., Gao Q., and Sun XF. (1996) Fatigue Fract Eng Mater Struc, **19**, 839–854.
12. Fatemi A. and Socie DF. (1988) Fatigue Eng Mater Struct, **11**, 149–165.
13. Chen X., Xu S. and Hung DX. Proc. 7th Int. Fatigue Cong., 959–64.
14. McDowell DL., Stahl OK., Stock SR., and Antolovich S.D. Metallurgical and Materials Transactions A, **19**, 1277-1293.
15. Borodii MV. and Shukaev SM. (2007) Int J Fatigue, **29**, 1184-1191.
16. Kallmeyer AR., Krgo A., and Kurath P. (2001) Eng Mat Tech, **124**, 229-237.
17. Kallmeyer AR. and Kurath, P. (2006) AFRL-ML-WP-TR-2006-4112.